RESEARCH MEMORANDUM

EVALUATION OF FIVE CONICAL CENTER-BODY SUPERSONIC DIFFUSERS AT SEVERAL ANGLES OF ATTACK

By Gerald W. Englert and Leonard J. Obery

Lewis Flight Propulsion Laboratory
Cleveland, Ohio

NATIONAL ADVISORY COMMITTEE
FOR AERONAUTICS

WASHINGTON
May 5, 1952

319.98/13

NATIONAL ADVISORY COMMITTEE FOR AERONAUTICS

RESEARCH MEMORANDUM

EVALUATION OF FIVE CONICAL CENTER-BODY SUPERSONIC DIFFUSERS AT SEVERAL ANGLES OF ATTACK

By Gerald W. Englert and Leonard J. Obery

SUMMARY

Five supersonic inlets having conical center bodies were investigated on a 16-inch ram-jet engine with and without combustion at free-stream Mach numbers of 1.7, 1.9, and 2.0 and at angles of attack from 0° to 10°. Four of the inlets were of the low-mass-flow-ratio type (the angles of the oblique shock emanating from the center body were substantially greater than the angle between the model center line and the lines from the cone apex to the cowl lips). The fifth inlet was of the high-mass-flow-ratio type. An investigation of the effects of cone angle and cone surface boundary-layer bleed indicated that the stable operating range of the four low-mass-flow-ratio inlets decreased considerably as the angle of attack was increased from 0° to 6° despite an increase of the cone angle or the use of boundary-layer bleed. The stable range of the high mass-flow-ratio inlet increased considerably both at 0° and at greater angles of attack as the free-stream Mach number was decreased.

Free-stream Mach number, angle of attack, and inlet type had negligible effects on combustion efficiency, temperature ratio, or combustion-chamber inlet Mach number in the supercritical region. Total body drag decreased with an increase in the amount of heat added in the combustion chamber. This decrease appears to be due mainly to a decrease of pressure drag on the boattail-type exhaust nozzle with increased exit jet temperature.

INTRODUCTION

Increasing the center body cone angle of a supersonic inlet at 0° angle of attack decreases the Mach number in the flow field in which the inlet-terminal shock occurs. It is possible to decrease the pressure gradient across the shock to a value below which separation from the cone surface by this means will not occur (references 1 and 2). In cases where separation does occur, however, removal of this low energy air by means of a boundary-layer bleed system (references 2 to 4) can be effective in increasing the stable operating range of low-mass-flow-ratio

inlets (inlets for which the oblique shock emanating from the center body is substantially greater than the angles between the model center line and the line from the cone apex to the cowl lip).

Results of an investigation of the effectiveness of these two methods for increasing the stable operating range of low mass-flow-ratio inlets at angles of attack up to 10° made at the NACA Lewis laboratory are presented herein. These results are compared with the results of reference 2.

The investigation was conducted by use of a 16-inch ram-jet engine installed in the NACA Lewis 8- by 6-foot supersonic wind tunnel. The engine was used both with and without combustion to study the effect of inlet conditions on burner operation. Data were obtained at free-stream Mach numbers of 1.7, 1.9, and 2.0, and at Reynolds numbers, based on the model inlet diameter, of approximately 3.5 to 4×10^6.

APPARATUS AND PROCEDURE

A sketch of the configuration (a 16-in. Rigel ram jet) used for the noncombustion phase of the investigation is shown in figure 1(a). The inlets were detachable at station Y. Downstream of station Y, the engine and the instrumentation were the same as those reported in reference 1. Static pressure taps were located on the outer cowl surface. The coordinates of these taps and the corresponding measured static pressures for various mass flows and at several angles of attack are presented in table I.

For the combustion investigations, the straightening vanes downstream of station 3, the static-pressure survey tubes at station 4, and the mass-flow control plug were removed and a combustor and a 16-tube water-cooled total-pressure rake were installed as shown in the sketch in figure 1(b). The combustor consisted of a single ring annular V-gutter flame holder and four fuel manifolds each containing three spring-loaded fuel nozzles which sprayed normal heptane upstream. Two exhaust nozzles, having exit areas equal to 50 and 55 percent of the combustion chamber area, respectively, were used.

The inlets (fig. 2) investigated were the same as those discussed in references 1 and 3. All five inlets had conical projecting center bodies and very nearly the same mass flows at supercritical conditions. The inlets are identified by the cone half angle and the angle between the line from the apex of the cone to the cowl lip and the engine axis of symmetry. Inlets 20-27.4, 25-31.9, and 25-43.1 are described in detail in reference 1 and inlets 20-26.2 and 20-26.0 in reference 3. Inlets 20-26.2 and 20-26.0 had scoop-type boundary-layer bleed slots located 12 inches downstream of the center body apex. The bleed ducts discharged

at both sides of the model behind two small windshields. Four of these inlets were low-mass-flow-ratio inlets. The fifth inlet (inlet 25-43.1), however, was a high-mass-flow-ratio type; that is, at a free-stream Mach number of 2.0, a free-stream tube having a diameter equal to the cowl-lip diameter was swallowed at the critical mass-flow ratio.

A 0.375-inch-diameter pitot tube, the axis of symmetry of which coincided with that of the engine, extended $4\frac{1}{2}$ inches upstream of the cone apexes of all inlets. The effects of this tube on the characteristics of the inlets were assumed negligible.

The methods of data reduction for the noncombustion investigations are described in reference 1. The mass flow for the combustion investigations was computed from pressure instrumentation at stations 2 and X. The total temperature at the choked exit nozzle was computed from the total pressure measured at station 6 in conjunction with the measured mass flow.

RESULTS AND DISCUSSION

Noncombustion Operation

The variation of diffuser total-pressure ratio with mass-flow ratio of the five inlets at angles of attack from 0° to 10° and at Mach numbers of 1.7, 1.9, and 2.0 is shown in figure 3. Mass-flow ratio is defined herein as the ratio of the mass flow through the engine at any test condition to the mass flow through a free-stream tube having a diameter equal to the cowl-lip diameter. Diffuser total pressure ratio is defined as the total pressure at station 3 (fig. 2) divided by free-stream total pressure. The curves at 0° angle of attack were obtained from references 1 and 3. Solid lines denote stable operation and dashed lines denote pulsing regions.

In general, total-pressure ratio, critical mass-flow ratio, and the stable range of operation of the low-mass-flow-ratio inlets decreased with an increase of angle of attack from 0° to 6°. With increasing Mach number, the critical mass-flow ratio increased and the total-pressure ratio and the stable operating range decreased for the five inlets.

The stability of low-mass-flow-ratio inlets is associated with flow separation from the center-body surface (references 1 to 4). This separation depends on the static-pressure gradient in the boundary layer in the flow direction. A high static-pressure gradient can be imposed on the cone boundary layer by the presence of the inlet terminal shock. Increasing the upstream cone-surface Mach number increases the pressure gradient across the inlet terminal shock associated with subcritical operation and eventually causes separation. The Mach number at the outer

edge of the boundary layer on the top surface of the cone increases rapidly with free-stream Mach number and angle of attack as shown in figure 4. For instance, the Mach number on the top side of the 20° half-angle cone at a free-stream Mach number of 1.7 and 10° angle of attack is nearly equal to the Mach number on this same cone at a free-stream Mach number of 1.9 and zero angle of attack. The pressure gradient across the terminal shock at these two Mach numbers would then be nearly the same and the susceptibility of the cone-surface boundary layer to separation would be expected to be the same at these two points. Figures 3(a) and 3(f) show that the stability ranges of inlet 20-27.4 at these two conditions are of comparable magnitude. This relation can be more clearly demonstrated by a plot of the stable operating range as a function of cone-upper-surface Mach number for inlets 20-27.4 and 25-31.9 as shown in figure 5. Some of the data scatter may be due to variation in the angle between the terminal shock and the cone surface causing variation in static-pressure rise across the shock pattern even though upstream Mach number is the same. This analysis also indicates that a disturbance or region of low energy air on only one circumferential portion of the inlet (the upper surface for positive angles of attack) is sufficient to cause pulsing, which agrees with reference 2.

This phenomenon is also demonstrated by the schlieren photograph of figure 6(a), which was taken at the minimum stable mass flow to show the flow mechanism just before pulsing occurred. The inlet is at an angle of attack of 6° and at a free-stream Mach number of 1.7. A large region of separation originates from the intersection of the inlet terminal shock with the boundary layer on the upper surface of the cone, whereas no separated regions are detectable on the lower surface of the cone.

The action of the boundary-layer bleed apparatus of inlets 20-26.2 and 20-26.0 at zero angle of attack is demonstrated in figures 6(b), (c), and 6(d), (e), respectively. These figures show that there is a region upstream of the boundary-layer bleed gap in which the terminal shock can be located so that the bleed gap can handle the major portion of the separated air. This low-energy air is thus prevented from entering the engine and results in an increased subcritical stable range. When the terminal shock is located upstream of this region, the boundary-layer bleed system can no longer handle the large amounts of separated air and instability occurs (reference 3).

This boundary-layer bleed system, designed for zero angle of attack, became ineffective at high angles of attack. Instability occurred before the mass flow could be lowered sufficiently to push the terminal shock upstream of the boundary-layer bleed slot at an angle of attack of 6° and a free-stream Mach number of 2.0 (figs. 6(f) and 6(g)). The separated air originating from the intersection of the terminal shock with the boundary layer on the cone could not be swallowed by the bleed system and the low-energy air was permitted to enter the model for these conditions.

The boundary-layer bleeds could serve merely to reduce the boundary layer before the point of separation. It then appears that a boundary-layer bleed system must be designed for the angle of attack at which the inlet is to be operated.

With the high mass-flow inlet 25-43.1, instability occurred at free-stream Mach numbers of 1.9 and 2.0 in accordance with reference 2. According to reference 2, instability occurs when the vortex sheet generated by the intersection of the inlet terminal shock with the cone oblique shock enters the inlet at a radius slightly less than the cowl lip radius (fig. 6(h) and 6(i)). At a free-stream Mach number of 1.7, instability did not occur at zero angle of attack regardless of how close this vortex sheet came to the inner cowl surface. This result may be due to the weakness of the vortex sheet at this low Mach number.

The measured frequency and amplitude of pulsation are presented in figure 7 as a function of mass-flow ratio for inlets 20-27.4, 20-26.2, and 25-43.1 for various free-stream Mach numbers and angles of attack. Frequencies up to 12 cycles per second and amplitude coefficients (differences between maximum and minimum static pressures at station 3 divided by the free-stream dynamic pressure) as high as 1.6 were observed. Although no consistent variation of frequency with free-stream Mach number and angle of attack was apparent, the amplitude coefficient for all inlets generally increased with free-stream Mach number regardless of angle of attack.

Combustion Operation

Representative plots of the velocity distribution at the combustion chamber entrance (station 3) are given in figures 8 and 9. Curves of velocity ratio (ratio of local velocity to the maximum velocity in the flow channel) against radius ratio (ratio of radius at any point divided by the radius to the outer casing) are presented. All these curves are of similar form with the vertex occurring between radius ratios of 0.74 to 0.80. The free-stream Mach number and the various inlet configurations have little effect on velocity distribution throughout the stable mass-flow range. In general, with any given inlet, lower velocities occurred near the inner and outer walls during the combustion investigations than during the noncombustion investigation. The contribution of this flame holder and fuel jets could not be separated from the effects of heat addition. No consistent trend for angle of attack was obtained.

Typical combustor operating characteristics are presented in figures 10 and 11. The combustion efficiency (heat added to air/available heat in fuel), total-temperature ratio across the combustion chamber, and Mach number at the combustion-chamber entrance are plotted as a function of fuel-air ratio for several inlets, jet nozzle sizes, free-stream Mach numbers, and angles of attack.

The efficiency of the combustor, a scaled-down version of a successful 28-inch-diameter combustor (reference 5), was generally very poor. Because inlet evaluation was the primary object of this investigation, development of a more satisfactory combustor was not undertaken.

Blow-out occurred in all the combustion runs almost as soon as subcritical operation was attempted. The combustion data presented are therefore for supercritical mass-flow conditions only. These data indicate that variation in free-stream Mach number from 1.7 to 2.0 and in exit area ratio from 0.50 to 0.55 had little effect on the combustion efficiency and the temperature ratio. A single curve can be drawn through all the data for the 20° cone-half-angle inlets. In addition, increases in the angle of attack from 0° to 6° caused no change in combustor operation or performance.

Because the combustor performance was poor, no over-all engine efficiency or propulsive thrust data are presented. However, a reduction in external body drag with increasing combustion-chamber temperature similar to that reported in reference 6 was observed during these tests. Drag is defined herein as the resultant of all forces acting in directions parallel to the flight direction and acting external to the outermost stream lines entering and leaving the engine.

Drag reductions as high as 45 percent of the noncombustion value were observed at a stream Mach number of 2.0 (fig. 12).

This phenomenon may be due to the test techniques employed in obtaining the data and possibly may not be encountered in flight. Additional information is needed to determine the mechanism of the flow by which this effect occurs.

SUMMARY OF RESULTS

For the four low-mass-flow-ratio inlets (inlets for which the angle of the oblique shock emanating from the center body is substantially greater than the angle between the model center lines and the line from the cone apex to the cowl lip) and the high-mass-flow-ratio inlet considered, the following characteristics were observed:

1. The stable operating range of the low-mass-flow-ratio inlets decreased considerably as the angle of attack was increased from 0° to 6° despite an increase of the center body cone angle or the use of a boundary-layer bleed. The stable range of the high-mass-flow-ratio inlet at angles of attack from 0° to 6° increased considerably as the free-stream Mach number was decreased.

2. All the curves of combustion-chamber velocity ratio plotted against radius ratio were of similar form with the vertex at nearly the same radius ratio. In the stable operating range, these curves were fairly independent of inlet type, free-stream Mach number, and mass-flow ratio.

3. Free-stream Mach number, angle of attack, and inlet type had negligible effect on combustion efficiency, temperature ratio, and combustion-chamber inlet Mach number for the low-mass-flow-ratio inlets. The high-mass-flow-ratio inlet was not investigated with heat addition.

4. A decrease in the total body drag was obtained for an increase in the amount of heat added in the combustion chamber. Additional information is needed to determine the physical mechanism of the flow by which this effect occurs.

Lewis Flight Propulsion Laboratory
National Advisory Committee for Aeronautics
Cleveland, Ohio

REFERENCES

1. Nussdorfer, Theodore J., Obery, Leonard J., and Englert, Gerald W.: Pressure Recovery Drag, and Subcritical Stability Characteristics of Three Conical Supersonic Diffusers at Stream Mach Numbers from 1.7 to 2.0. NACA RM E51H27.

2. Ferri, Antonio, and Nucci, Louis M.: The Origin of Aerodynamic Instability of Supersonic Inlets at Subcritical Condition. NACA RM L50K30, 1951.

3. Obery, Leonard J., Englert, Gerald W., and Nussdorfer, Theodore J.: Pressure Recovery, Drag, and Subcritical Stability Characteristics of Conical Supersonic Diffusers with Boundary-Layer Removal. NACA RM E51H29.

4. Fisher, R. E.: Controlling the Subcritical Stability of Conical Shock Inlets. Marquardt Aircraft Co. Presented at the symposium on the Aerodynamics of Ramjet Supersonic Inlets (Wright-Patterson Air Force Base, Dayton), Oct. 3 and 4, 1950.

5. Shillito, T. B., and Nakanishi, Shigeo: Effect of Design Changes and Operating Conditions on Combustion and Operational Performance of a 28-Inch Diameter Ram-Jet Engine. NACA RM E51J24.

6. Perchonok, Eugene, Wilcox, Fred, and Pennington, Donald: Effect of Angle of Attack and Exit Nozzle Design on the Performance of a 16-Inch Ram Jet at Mach Numbers Between 1.5 and 2.0. NACA RM E51G26, 1951.

[redacted]

TABLE I - EXTERNAL PRESSURE DISTRIBUTION ON 16-INCH RIGEL RAM-JET ENGINE FOR SEVERAL ANGLES OF ATTACK

(a) Angle of attack, 0°; free-stream Mach number, 1.70.

Distance from cowl lip (in.)	Inlet									
	20-27.4		20-26.2		20-26.0		25-31.9		25-43.1	
	Circumferential position[a]									
	191°	349°	191°	349°	191°	349°	191°	349°	191°	349°
	Mass-flow ratio									
	0.595		0.534		0.476		0.535		0.907	
0.5	0.8065	0.8126	0.657	0.706	0.5736	0.5197	0.5870	0.5930	0.797	0.754
1.0	.7644	.7214	.614	.664	.5436	.5077	.5810	.5930	.693	.705
1.5	.6913	.6432	.608	.620	.5256	.5376	.5870	.5630	.852	.723
2.0	.3164	.3465	.106	.118	.0676	.0736	.1105	.1165	.301	.259
3.0	.3044	.2923	.014	.021	-.0171	-.0171	.0266	.0326	.204	.204
4.0	-------	.1410	-.053	-.053	-.0634	-.0711	-.0103	-.0034	.124	.112
5.0	-.05933	-.05933	.002	-.065	-.0531	-.0651	-.0583	-.0463	.094	.069
7.0	-.08341	-.08341	-.053	-.041	-.0471	-.0351	-.0703	-.0643	.045	.045
10.0	-.04729	-.05331	-.047	-.029	-.0231	-.0137	-.0463	.0343	.039	.051
14.0	-.01032	-.02923	-.029	-.017	-.0291	-.0231	-.0223	.0026	.051	.057
18.0	-.01634	-.02322	-----	-----	------	------	-.0034	-.0103	.063	.051
22.0	-------	-------	-----	-----	------	------	------	------	.063	.051
	Mass-flow ratio									
	0.497		0.355		0.263		0.302		0.587	
0.5	0.5350	0.5650	0.161	0.154	0.0086	-0.0222	0.0145	0.0205	0.116	0.128
1.0	.6256	.5897	.296	.346	.1343	.1223	.1403	.1343	.287	.299
1.5	.6077	.5709	.383	.389	.2130	.2250	.2429	.2070	.552	.434
2.0	.2829	.3188	.013	.019	-.0642	-.0582	-.0582	-.0582	.178	.147
3.0	.2761	.2641	-.043	-.037	-.1061	-.1061	-.1061	-.0881	.141	.141
4.0	-------	.1197	-.111	-.092	-.1300	-.1300	-.1061	-.1061	.074	.068
5.0	-.07265	-.07265	-.104	-.098	-.1121	-.1180	-.1300	-.1180	.056	.037
7.0	-.09658	-.09060	-.080	-.080	-.0941	-.0821	-.1180	-.1061	.012	.012
10.0	-.05470	-.06068	-.061	-.043	-.0582	-.0522	-.0761	-.0582	.019	.025
14.0	-.01795	-.03675	-.049	-.031	-.0462	-.0402	-.0402	-.0342	.031	.037
18.0	-.01795	-.03077	-----	-----	------	------	-.0163	-.0222	.049	.037
22.0	-------	-------	-----	-----	------	------	------	------	.056	.037

[a]Measured in a counterclockwise direction when facing front of engine, 90° at top of engine.

2324

TABLE I - EXTERNAL PRESSURE DISTRIBUTION ON 16-INCH RIGEL RAM-JET ENGINE FOR SEVERAL ANGLES OF ATTACK - Continued

(b) Angle of attack, 3°; free-stream Mach number, 1.70.

Distance from cowl lip (in.)	Inlet									
	20-27.4		20-26.2		20-26.0		25-31.9		25-43.1	
	Circumferential position[a]									
	191°	349°	191°	349°	191°	349°	191°	349°	191°	349°
	Mass-flow ratio									
	0.592		0.533		-----		0.534		-----	
0.5	-----	-----	0.494	0.823	-----	-----	0.4433	0.7277	-----	-----
1.0	0.560	0.846	.481	-----	-----	-----	.4742	.6976	-----	-----
1.5	.217	.725	.487	.725	-----	-----	.4863	.6615	-----	-----
2.0	.236	.395	.042	.158	-----	-----	.0507	.1598	-----	-----
3.0	.230	.357	-.043	.061	-----	-----	-.0284	.0687	-----	-----
4.0	-----	.198	-.104	-.019	-----	-----	-.0524	.0326	-----	-----
5.0	-.101	-.012	-.080	-.025	-----	-----	-.1005	-.0163	-----	-----
7.0	-.120	-.037	-.092	-.007	-----	-----	-.1065	-.0284	-----	-----
10.0	-.107	-.006	-.074	.024	-----	-----	-.0825	-.0034	-----	-----
14.0	-.043	.014	-.055	.024	-----	-----	-.0524	.0086	-----	-----
18.0	-.031	.014	-----	-----	-----	-----	-.0284	.0146	-----	-----
22.0	-----	-----	-----	-----	-----	-----	------	------	-----	-----
	Mass-flow ratio									
	0.530		0.431		0.350		0.408		0.651	
0.5	0.382	0.934	0.185	0.591	0.045	0.279	0.0747	0.4433	0.080	0.426
1.0	.433	.852	.277	.690	.128	.400	.1538	.5524	.220	.658
1.5	.439	.725	.346	.678	.189	.491	.2380	.5885	.451	.695
2.0	.192	.395	-.006	.142	-.088	.068	-.0704	.1389	.116	.238
3.0	.186	.357	-.073	.056	-.136	-.010	-.1186	.0507	.086	.220
4.0	-----	.198	-.135	-.024	-.161	-.046	-.1366	.0206	.031	.134
5.0	-.113	-.012	-.135	-.031	-.142	-.034	-.1615	-.0223	.012	.098
7.0	-.126	-.037	-.104	-.012	-.112	-.004	-.1546	-.0344	-.018	.074
10.0	-.113	-.006	-.086	.025	-.088	.015	-.1125	-.0034	-.012	.080
14.0	-.050	.014	-.061	.025	-.064	.009	-.0644	.0086	.006	.080
18.0	-.044	.014	-----	-----	-----	-----	-.0344	.0146	.031	.074
22.0	-----	-----	-----	-----	-----	-----	------	------	.037	.074

[a]Measured in a counterclockwise direction when facing front of engine, 90° at top of engine.

TABLE I - EXTERNAL PRESSURE DISTRIBUTION ON 16-INCH RIGEL RAM-JET ENGINE FOR SEVERAL ANGLES OF ATTACK - Continued

(c) Angle of attack, 6°; free-stream Mach number, 1.70.

Distance from cowl lip (in.)	Inlet									
	20-27.4		20-26.2		20-26.0		25-31.9		25-43.1	
	Circumferential position[a]									
	191°	349°	191°	349°	191°	349°	191°	349°	191°	349°
	Mass-flow ratio									
	0.592		0.535		0.469		0.520		0.886	
0.5	-----	-----	0.380	0.941	0.352	0.749	0.2984	0.8413	0.390	0.950
1.0	0.408	0.922	.373	.855	.322	.707	.3465	.7993	.402	.864
1.5	.401	.788	.386	.825	.322	.737	.3765	.7513	.621	.822
2.0	.161	.433	-.017	.179	-.052	.159	-.0163	.1955	.164	.286
3.0	.153	.401	-.090	.093	-.124	.068	-.0883	.1106	.104	.329
4.0	-----	.236	-.158	.020	-.161	.015	-.1063	.0746	.031	.232
5.0	-.138	.027	-.158	.020	-.142	.021	-.1484	.0326	.006	.183
7.0	-.145	.002	-.127	.044	-.124	.056	-.1484	.0146	-.030	.140
10.0	-.132	.027	-.108	.062	-.094	.074	-.1123	.0446	-.024	.128
14.0	-.069	.046	-.078	.062	-.070	.056	-.0763	.0506	-.006	.128
18.0	-.050	.059	-----	-----	-----	-----	-.0403	.0626	-.019	.116
22.0	-----	-----	-----	-----	-----	-----	------	------	.031	.116
	Mass-flow ratio									
	0.561		0.479		0.413		0.452		0.771	
0.5	-----	-----	0.170	0.942	0.074	0.735	0.0805	0.8406	0.080	0.925
1.0	0.956	0.923	.231	.856	.115	.687	.1345	.7986	.201	.852
1.5	.981	1.171	.285	.825	.164	.723	.2014	.7566	.444	.828
2.0	.758	.434	-.057	.176	-.107	.152	-.0943	.1954	.073	.280
3.0	.758	.409	-.112	.096	-.162	.062	-.1362	.1105	.037	.323
4.0	-----	.873	-.174	.023	-.185	.014	-.1542	.0146	-.018	.232
5.0	-.150	.034	-.174	.017	-.168	.020	-.1851	.0326	-.024	.183
7.0	-.150	.003	-.143	.041	-.149	.050	-.1791	.0146	-.048	.146
10.0	-.131	.028	-.112	.065	-.113	.068	-.1422	.0446	-.036	.128
14.0	-.068	.047	-.088	.059	-.083	.056	-.0883	.0566	-.012	.128
18.0	-.056	.066	-----	-----	-----	-----	-.0463	.0686	.012	.116
22.0	-----	-----	-----	-----	-----	-----	------	------	.025	.116

[a]Measured in a counterclockwise direction when facing front of engine, 90° at top of engine.

2324

TABLE I - EXTERNAL PRESSURE DISTRIBUTION ON 16-INCH RIGEL RAM-JET ENGINE FOR SEVERAL ANGLES OF ATTACK - Continued

(d) Angle of attack, 10°; free-stream Mach number, 1.70.

Distance from cowl lip (in.)	Inlet 20-27.4			
	Circumferential position[a]			
	191°	349°	191°	349°
	Mass-flow ratio			
	0.585		0.539	
0.5	0.2729	1.119	0.1959	1.131
1.0	.2907	.9881	.1959	.9991
1.5	.2907	.8508	.2257	.8612
2.0	.0754	.4814	.0281	.4898
3.0	.0695	.4873	.0221	.4957
4.0	------	.3144	------	.3220
5.0	-.1873	.0754	-.2061	.0818
7.0	-.1814	.0636	-.1942	.0698
10.0	-.1331	.0873	-.1457	.0937
14.0	-.0915	.0932	-.1039	.0937
18.0	-.0737	.0932	-.0741	.0997
22.0	------	------	------	------

[a]Measured in a counterclockwise direction when facing front of engine, 90° at top of engine.

TABLE I - EXTERNAL PRESSURE DISTRIBUTION ON 16-INCH RIGEL RAM-JET ENGINE FOR SEVERAL ANGLES OF ATTACK - Continued

(e) Angle of attack, 0°; free-stream Mach number, 2.0.

Distance from cowl lip (in.)	Inlet									
	20-27.4		20-26.2		20-26.0		25-31.9		25-43.1	
	Circumferential position[a]									
	191°	349°	191°	349°	191°	349°	191°	349°	191°	349°
	Mass-flow ratio									
	0.653		0.589		0.515		0.603		1.000	
0.5	0.680	0.680	0.595	0.577	0.541	0.466	0.554	0.566	0.668	0.657
1.0	.627	.622	.559	.585	.517	.460	.566	.554	.622	.628
1.5	.645	.593	.571	.559	.483	.489	.583	.531	.674	.634
2.0	.342	.371	.146	.140	.109	.103	.153	.159	.296	.285
3.0	.325	.482	.057	.051	.017	.017	.072	.067	.244	.238
4.0	-----	.161	-.019	-.013	-.029	-.029	.033	.027	.153	.147
5.0	-.007	-.013	-.038	-.032	-.023	-.034	-.013	-.013	.124	.107
7.0	-.049	-.049	-.025	-.019	-.029	-.023	-.030	-.030	.067	.072
10.0	-.037	-.031	-.025	-.002	-.023	-.006	-.030	-.013	.061	.061
14.0	-.007	-.013	-.019	-.008	-.017	-.011	-.013	-.007	.044	.050
18.0	-.007	-.013	-----	-----	-----	-----	.004	.004	.055	.050
22.0	-----	-----	-----	-----	-----	-----	-----	-----	.061	.050
	Mass-flow ratio									
	0.616		0.412		0.304		0.533		-----	
0.5	0.643	0.626	0.236	0.219	0.106	0.054	0.458	0.429	-----	-----
1.0	.609	.603	.358	.393	.214	.203	.498	.475	-----	-----
1.5	.603	.569	.423	.429	.278	.272	.544	.480	-----	-----
2.0	.340	.357	.085	.085	.026	.015	.143	.137	-----	-----
3.0	.318	.301	.016	.021	-.019	-.025	.068	.062	-----	-----
4.0	-----	.158	-.037	-.043	-.060	-.066	-.029	.028	-----	-----
5.0	-.013	-.013	-.049	-.043	-.060	-.066	-.012	-.012	-----	-----
7.0	-.047	-.053	-.049	-.043	-.060	-.049	-.035	-.035	-----	-----
10.0	-.030	-.036	-.043	-.025	-.037	-.025	-.029	-.018	-----	-----
14.0	-.007	-.019	-.031	-.019	-.031	-.025	-.012	-.007	-----	-----
18.0	-.013	-.013	-----	-----	-----	-----	-.001	-.001	-----	-----
22.0	-----	-----	-----	-----	-----	-----	-----	-----	-----	-----

[a]Measured in a counterclockwise direction when facing front of engine, 90° at top of engine.

2324

TABLE I - EXTERNAL PRESSURE DISTRIBUTION ON 16-INCH RIGEL RAM-JET FOR SEVERAL ANGLES OF ATTACK - Continued

(f) Angle of attack, 3°; free-stream Mach number, 2.0.

Distance from cowl lip (in.)	Inlet							
	20-27.4		20-26.2		20-26.0		25-31.9	
	Circumferential position[a]							
	191°	349°	191°	349°	191°	349°	191°	349°
	Mass-flow ratio							
	-----		0.589		-----		0.596	
0.5	-----	-----	0.466	0.705	-----	-----	0.438	0.666
1.0	-----	-----	.437	.705	-----	-----	.449	.649
1.5	-----	-----	.443	.658	-----	-----	.466	.626
2.0	-----	-----	.075	.209	-----	-----	.083	.214
3.0	-----	-----	-.006	.110	-----	-----	.009	.118
4.0	-----	-----	-.076	.035	-----	-----	-.025	.077
5.0	-----	-----	-.082	.023	-----	-----	-.066	.037
7.0	-----	-----	-.070	.029	-----	-----	-.071	.020
10.0	-----	-----	-.059	.035	-----	-----	-.066	.032
14.0	-----	-----	-.047	.023	-----	-----	-.043	.032
18.0	-----	-----	-----	-----	-----	-----	-.025	.032
22.0	-----	-----	-----	-----	-----	-----	-----	-----
	Mass-flow ratio							
	0.635		0.482		0.367		0.561	
0.5	0.495	0.798	0.209	0.594	0.075	0.358	0.307	0.667
1.0	.495	.711	.303	.681	.151	.444	.347	.650
1.5	.484	.676	.349	.634	.208	.502	.399	.627
2.0	.245	.432	.041	.192	-.028	.128	.055	.210
3.0	.216	.373	-.024	.110	-.080	.047	-.013	.119
4.0	-----	.222	-.088	.029	-.103	.007	-.042	.072
5.0	-.069	.031	-.088	.017	-.092	.012	-.071	.038
7.0	-.086	.002	-.076	.029	-.080	.024	-.082	.015
10.0	-.063	.013	-.065	.035	-.069	.024	-.071	.032
14.0	-.039	.013	-.059	.023	-.057	.012	-.042	.027
18.0	-.033	.007	-----	-----	-----	-----	-.024	.027
22.0	-----	-----	-----	-----	-----	-----	-----	-----

[a]Measured in a counterclockwise direction when facing front of engine, 90° at top of engine.

TABLE I - EXTERNAL PRESSURE DISTRIBUTION ON 16-INCH RIGEL RAM-JET ENGINE FOR SEVERAL ANGLES OF ATTACK - Continued

(g) Angle of attack, 6°; free-stream Mach number, 2.0.

Distance from cowl lip (in.)	Inlet							
	20-27.4		20-26.2		20-26.0		25-31.9	
	Circumferential position[a]							
	191°	349°	191°	349°	191°	349°	191°	349°
	Mass-flow ratio							
	0.650		0.583		0.506		0.592	
0.5	-----	-----	0.359	0.883	0.304	0.685	0.342	0.807
1.0	0.392	0.887	.342	.824	.269	.672	.348	.790
1.5	.381	.779	.348	.784	.264	.697	.371	.756
2.0	.175	.494	.022	.273	-.020	.222	-.019	.280
3.0	.147	.432	-.054	.162	-.084	.119	-.030	.176
4.0	-----	.266	-.111	.080	-.118	.061	-.059	.130
5.0	-.099	.066	-.111	.063	-.101	.061	-.099	.084
7.0	-.116	.032	-.094	.069	-.095	.072	-.099	.061
10.0	-.110	.044	-.088	.080	-.078	.078	-.088	.067
14.0	-.065	.061	-.077	.074	-.067	.067	-.065	.067
18.0	-.053	.055	-----	-----	-----	-----	-.042	.067
22.0	-----	-----	-----	-----	-----	-----	-----	-----
	Mass-flow ratio							
	0.638		0.573		0.486		0.576	
0.5	0.423	0.963	0.320	0.886	0.197	0.688	0.237	0.809
1.0	.376	.870	.315	.827	.203	.676	.255	.786
1.5	.370	.793	.332	.781	.238	.694	.295	.752
2.0	.170	.505	.012	.274	-.033	.220	-.002	.278
3.0	.159	.441	-.053	.163	-.097	.117	-.060	.175
4.0	-----	.276	-.117	.075	-.120	.059	-.083	.129
5.0	-.100	.076	-.117	.064	-.108	.059	-.111	.083
7.0	-.106	.041	-.099	.070	-.097	.070	-.111	.060
10.0	-.106	.047	-.088	.081	-.085	.076	-.089	.071
14.0	-.065	.058	-.070	.075	-.074	.065	-.066	.071
18.0	-.053	.058	-----	-----	-----	-----	-.043	.071
22.0	-----	-----	-----	-----	-----	-----	-----	-----

[a] Measured in a counterclockwise direction when facing front of engine, 90° at top of engine.

TABLE I - EXTERNAL PRESSURE DISTRIBUTION ON 16-INCH RIGEL RAM-JET ENGINE FOR SEVERAL ANGLES OF ATTACK - Continued

(h) Angle of attack, 10°; free-stream Mach number, 2.0.

Distance from cowl lip (in.)	Inlet									
	20-27.4		20-26.0		25-31.9		20-26.0		25-31.9	
	Circumferential position[a]									
	191°	349°	191°	349°	191°	349°	191°	349°	191°	349°
	Mass-flow ratio									
	0.643		0.493		0.578		0.473		0.558	
0.5	0.281	1.189	0.143	0.871	0.200	1.006	0.096	0.870	0.178	1.007
1.0	.251	1.066	.132	.819	.212	.936	.096	.818	.218	.937
1.5	.263	.931	.155	.843	.252	.891	.120	.842	.265	.886
2.0	.092	.591	-.081	.292	-.035	.344	-.081	.292	-.023	.345
3.0	.075	.562	-.132	.189	-.093	.258	-.127	.182	-.087	.259
4.0	-----	.362	-.155	.126	-.110	.206	-.156	.125	-.109	.207
5.0	-.130	.128	-.143	.126	-.139	.149	-.144	.125	-.138	.150
7.0	-.142	.092	-.138	.143	-.145	.120	-.138	.143	-.144	.115
10.0	-.130	.105	-.121	.138	-.122	.132	-.116	.137	-.127	.132
14.0	-.083	.111	-.098	.115	-.093	.126	-.099	.114	-.092	.121
18.0	-.056	.099	-----	-----	-.059	.120	-----	-----	-.064	.103
22.0	-----	-----	-----	-----	-----	-----	-----	-----	-----	-----

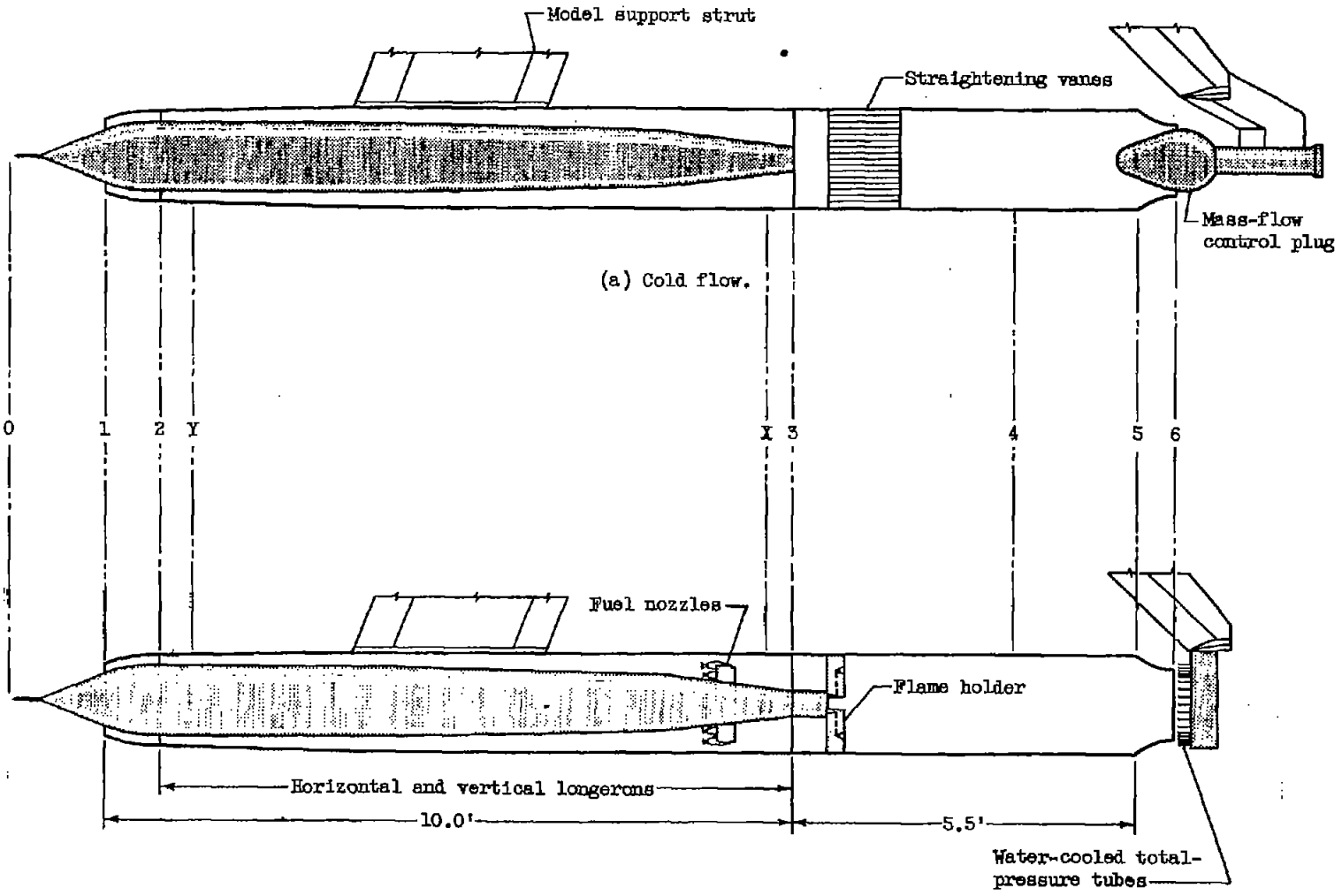

Figure 1. - Diagrammatic sketch of 18-inch ram-jet engine.

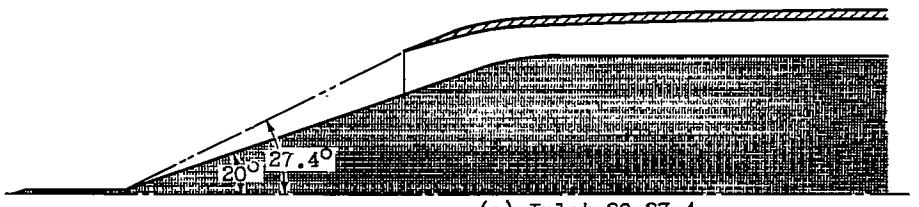

Free-stream Mach number	Ratio of maximum free-stream tube area to maximum area of engine
1.7	0.301
1.9	.321
2.0	.330

(a) Inlet 20-27.4.

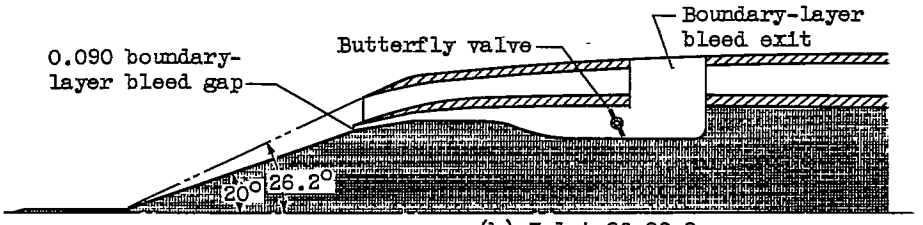

1.7	0.302
1.9	.324
2.0	.332

(b) Inlet 20-26.2.

1.7	0.283
1.9	.297
2.0	.306

(c) Inlet 20-26.0.

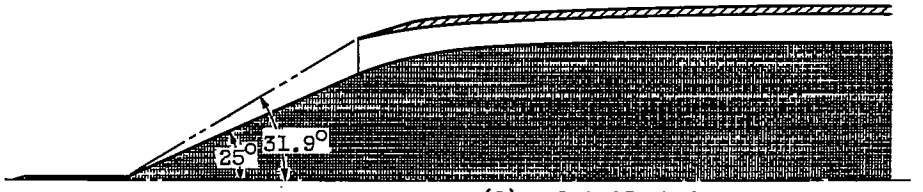

1.7	0.291
1.9	.317
2.0	.328

(d) Inlet 25-31.9.

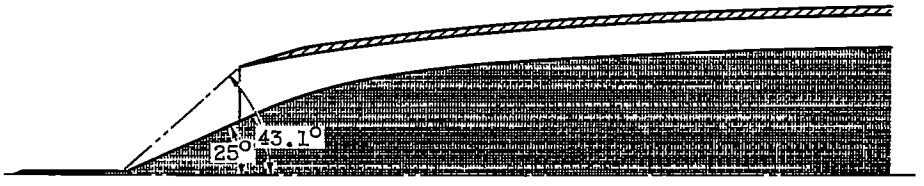

1.7	0.290
1.9	.313
2.0	.320

(e) Inlet 25-43.1.

Figure 2. - Geometric comparison of five inlets.

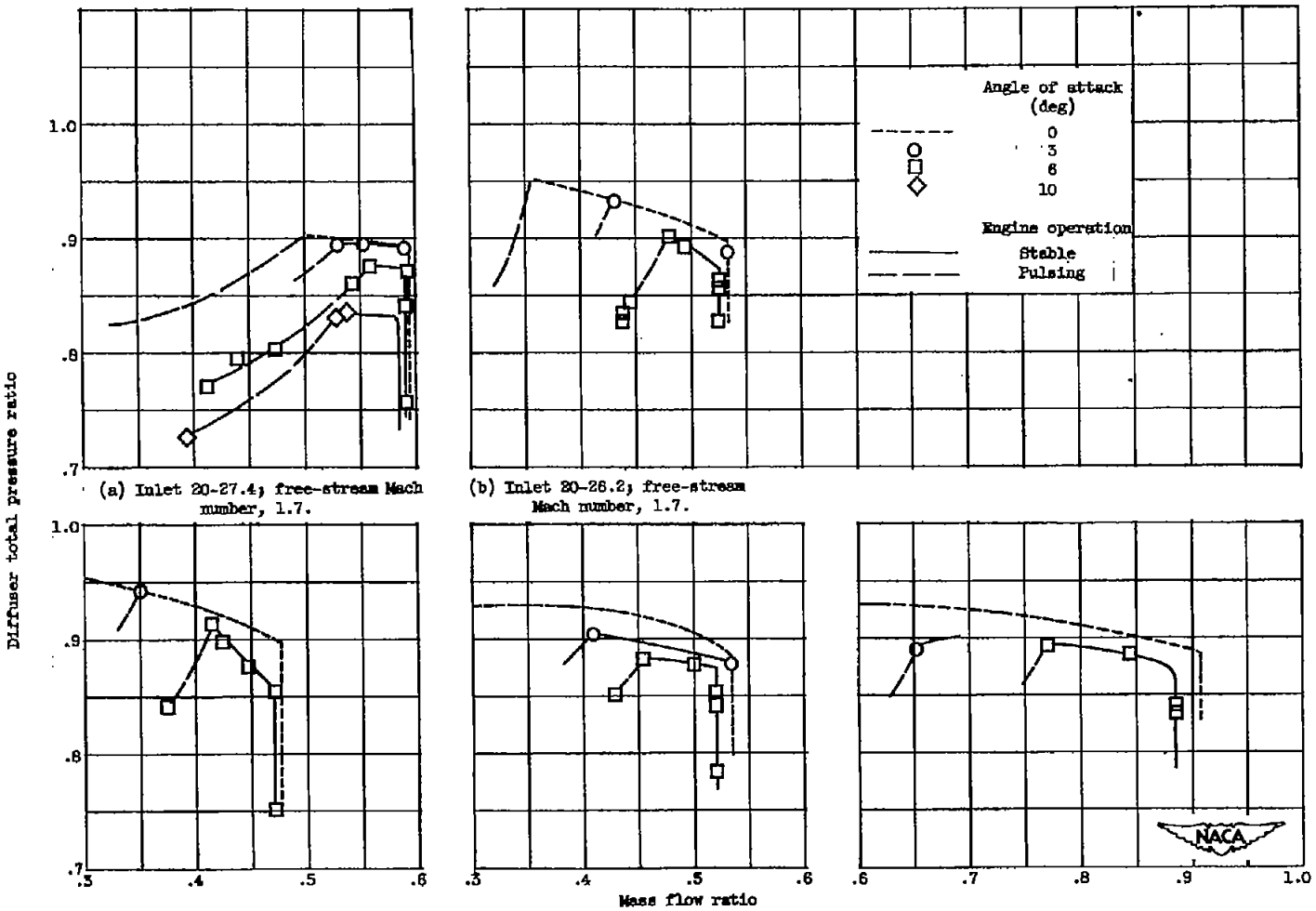

(a) Inlet 20-27.4; free-stream Mach number, 1.7.

(b) Inlet 20-26.2; free-stream Mach number, 1.7.

(c) Inlet 20-26.0; free-stream Mach number, 1.7.

(d) Inlet 25-31.9; free-stream Mach number, 1.7.

(e) Inlet, 25-43.1; free-stream Mach number, 1.7.

Figure 3. - Variation of diffuser pressure ratio with mass-flow ratio.

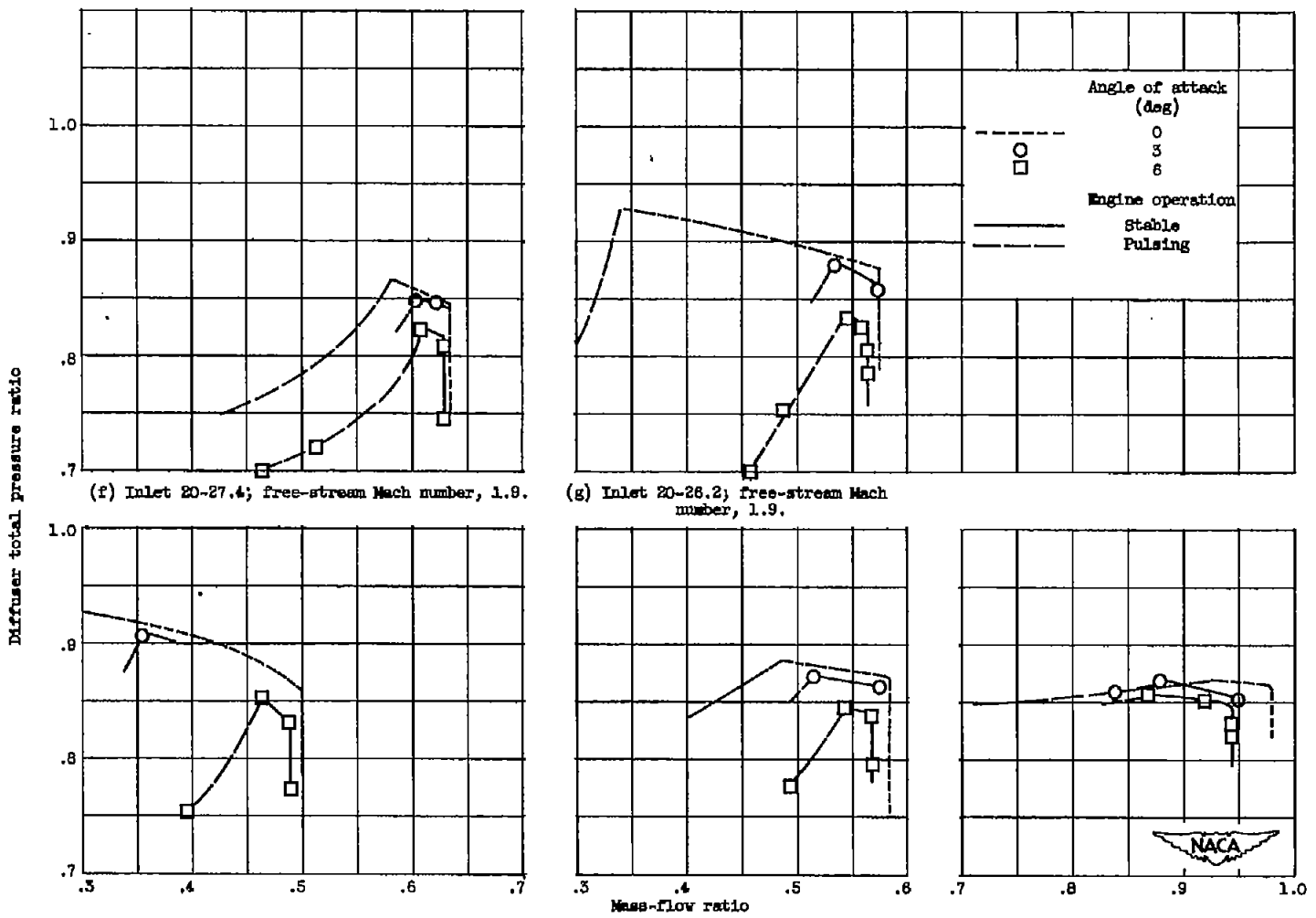

(f) Inlet 20-27.4; free-stream Mach number, 1.9.

(g) Inlet 20-26.2; free-stream Mach number, 1.9.

(h) Inlet 20-26.0; free-stream Mach number, 1.9.

(i) Inlet 25-31.9; free-stream Mach number, 1.9.

(j) Inlet 25-43.1; free-stream Mach number, 1.9.

Figure 3. - Continued. Variation of diffuser total pressure ratio with mass-flow ratio.

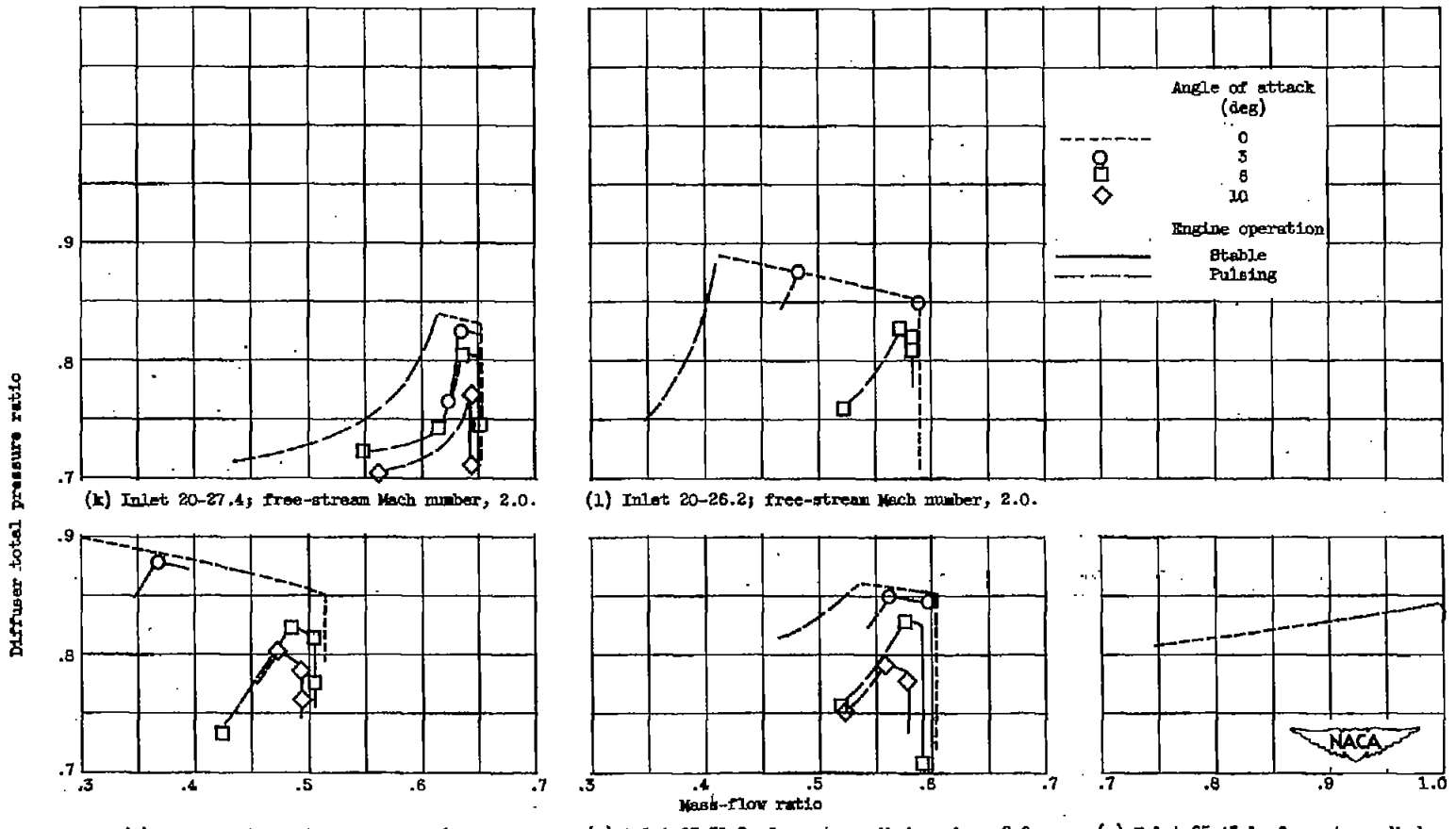

(k) Inlet 20-27.4; free-stream Mach number, 2.0.

(l) Inlet 20-26.2; free-stream Mach number, 2.0.

(m) Inlet 20-26.0; free-stream Mach number, 2.0.

(n) Inlet 25-31.9; free-stream Mach number, 2.0.

(o) Inlet 25-43.1; free-stream Mach number, 2.0.

Figure 3. - Concluded. Variation of diffuser total pressure ratio with mass-flow ratio.

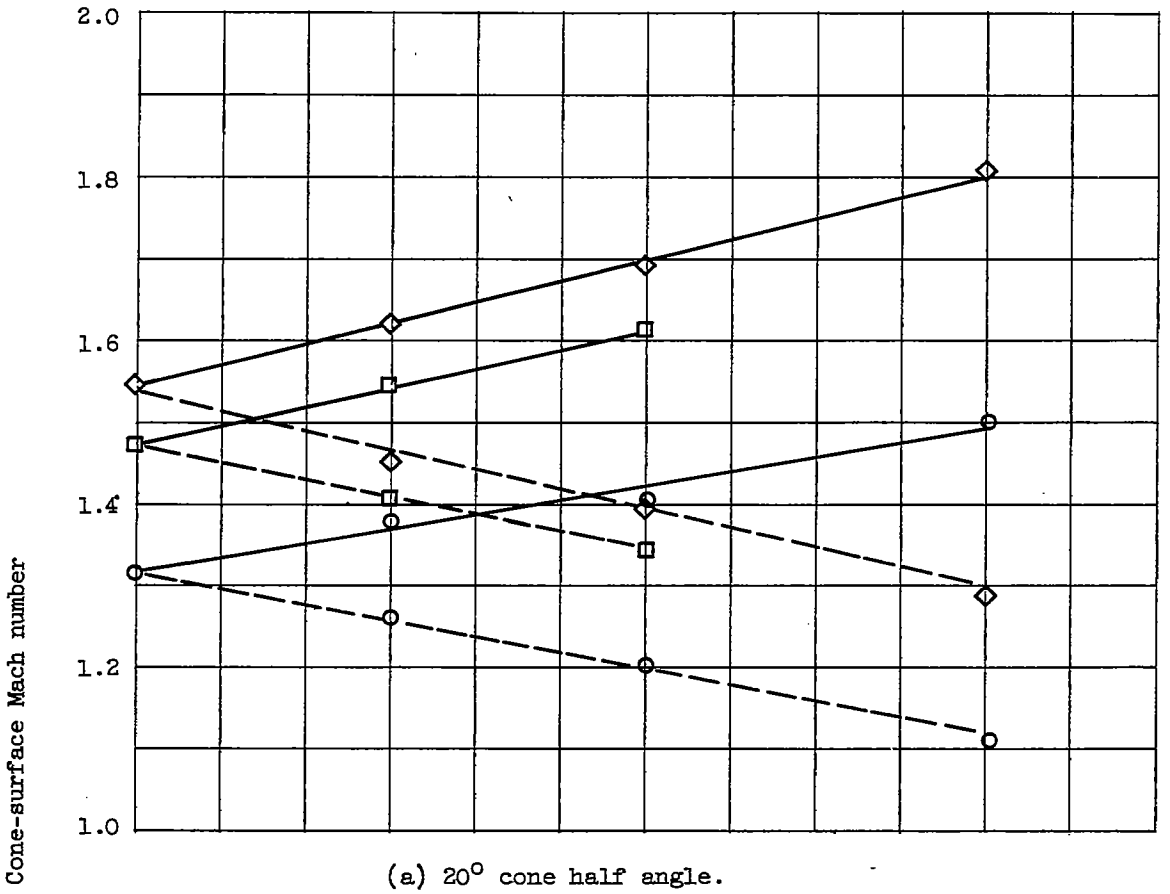

(a) 20° cone half angle.

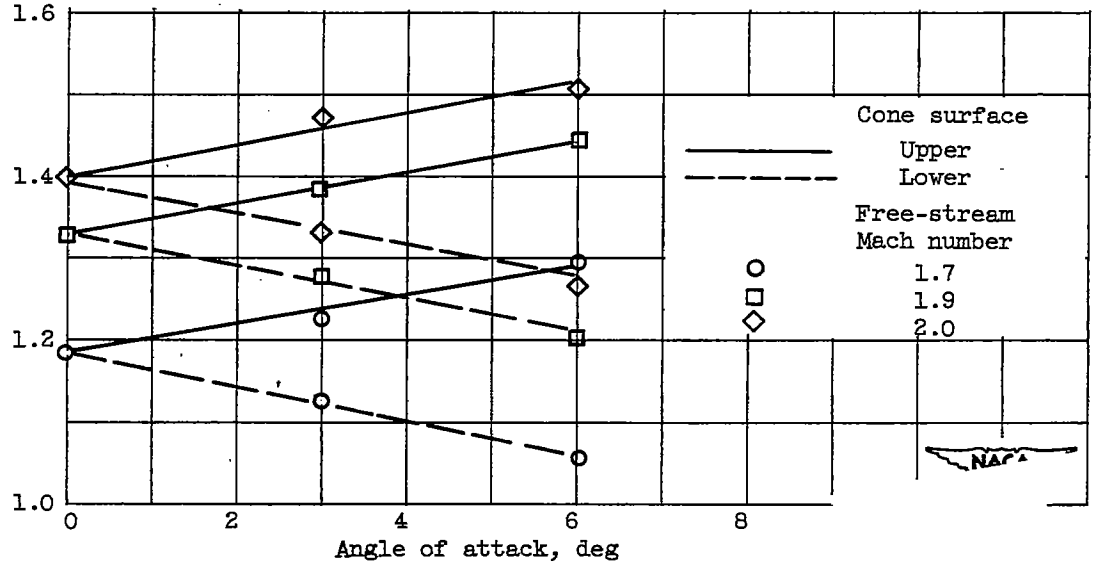

(b) 25° cone half angle.

Figure 4. - Variation of cone-surface Mach number with angle of attack.

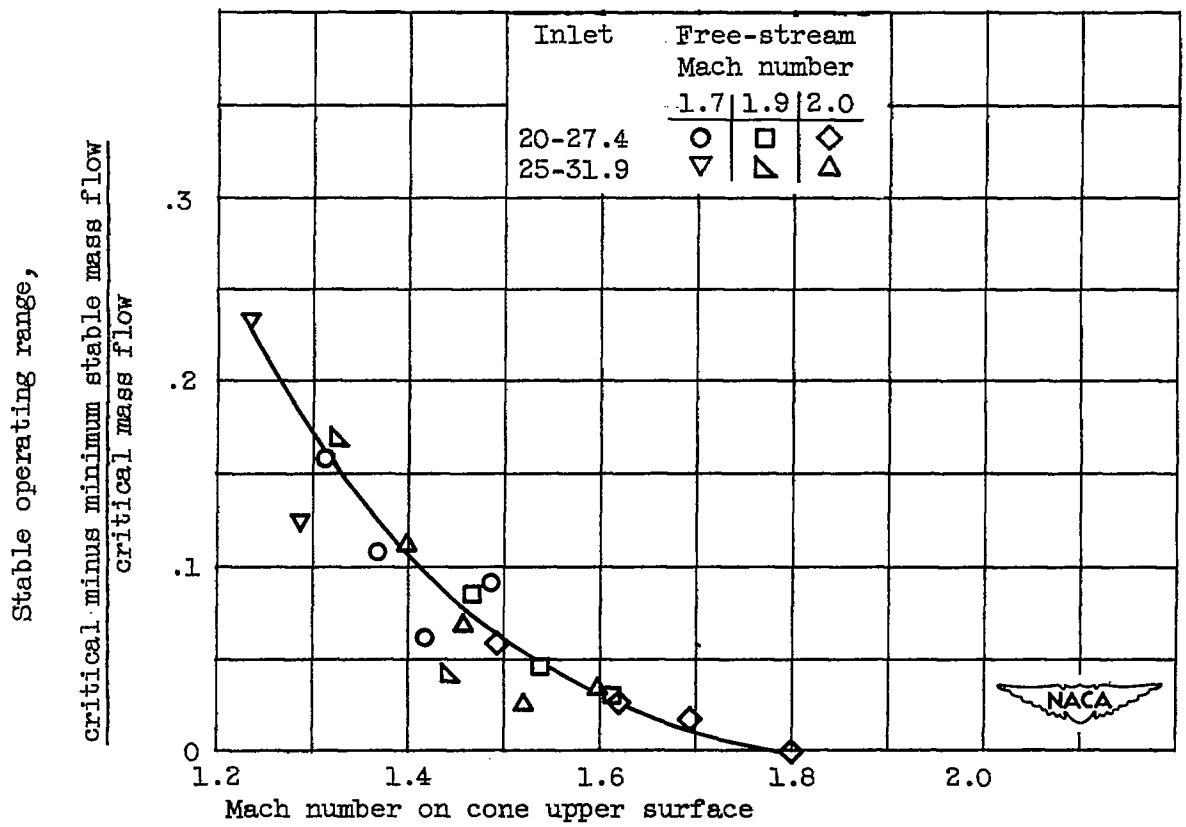

Figure 5. - Variation of stable operating range with Mach number on cone upper surface.

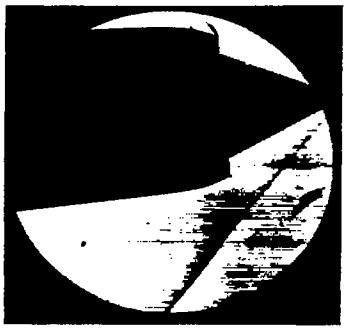

(a) Inlet, 25-31.9; free-stream Mach number, 1.7; angle of attack, 6°; mass-flow ratio, 0.452 (minimum stable).

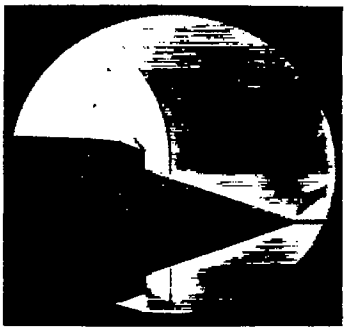

(b) Inlet, 20-26.2; free-stream Mach number, 1.7; angle of attack, 0°; mass-flow ratio, 0.355 (minimum stable).

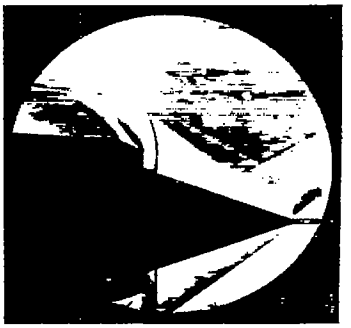

(c) Inlet, 20-26.2; free-stream Mach number, 2.0; angle of attack, 0°; mass-flow ratio, 0.412 (minimum stable).

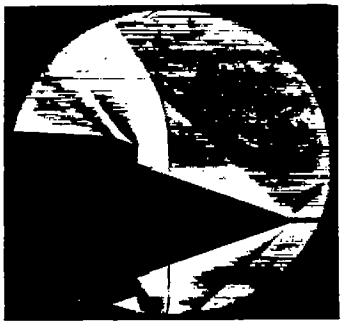

(d) Inlet, 20-26.0; free-stream Mach number, 1.7; angle of attack, 0°; mass-flow ratio, 0.263.

(e) Inlet, 20-26.0; free-stream Mach number, 2.0; angle of attack, 0°; mass-flow ratio, 0.304.

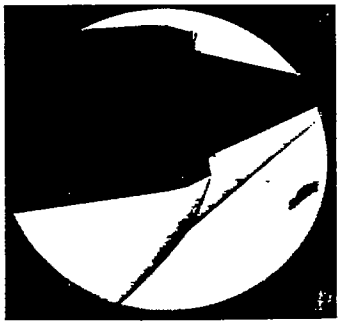

(f) Inlet, 20-26.2; free-stream Mach number, 2.0; angle of attack, 6°; mass-flow ratio, 0.573 (minimum stable).

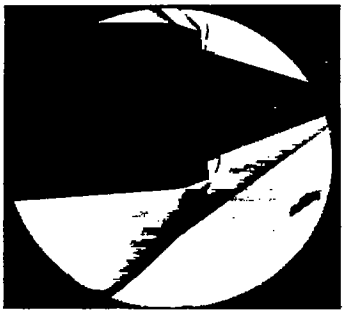

(g) Inlet, 20-26.0; free-stream Mach number, 2.0; angle of attack, 6°; mass-flow ratio, 0.486 (minimum stable).

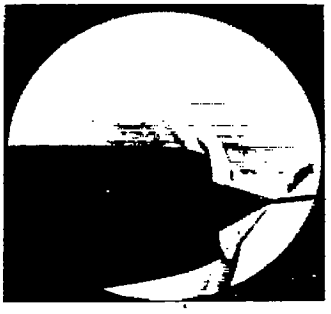

(h) Inlet, 25-43.1; free-stream Mach number, 1.7; angle of attack, 0°; mass-flow ratio, 0.736.

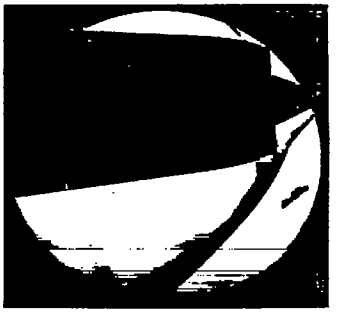

(i) Inlet, 25-43.1; free-stream Mach number, 1.7; angle of attack, 6°; mass-flow ratio, 0.771 (minimum stable).

Figure 6. - Schlieren photographs of external shock configuration. C-28894

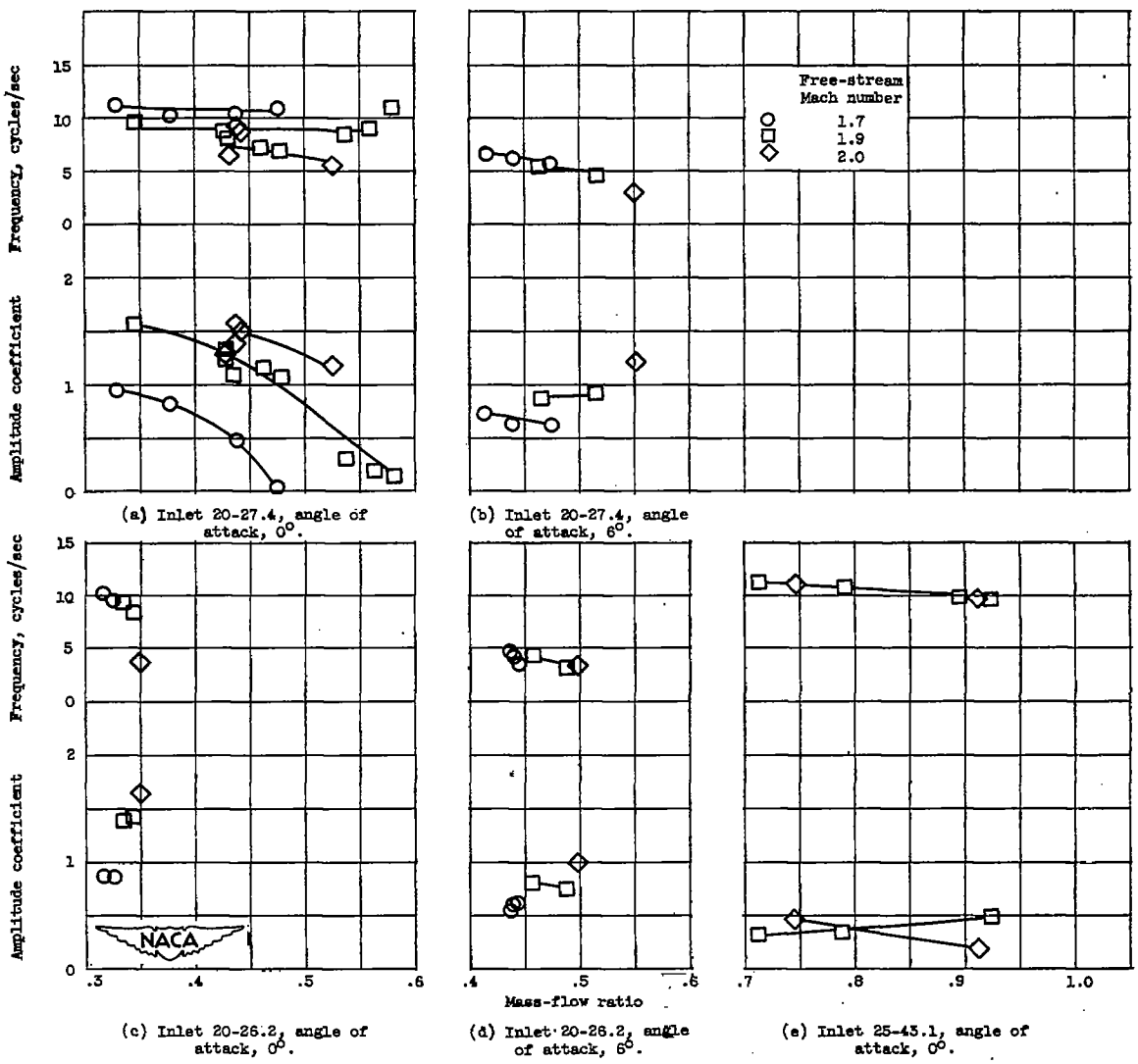

(a) Inlet 20-27.4, angle of attack, 0°.

(b) Inlet 20-27.4, angle of attack, 6°.

(c) Inlet 20-26.2, angle of attack, 0°.

(d) Inlet 20-26.2, angle of attack, 6°.

(e) Inlet 25-43.1, angle of attack, 0°.

Figure 7. - Variation of frequency and amplitude of pulsing with mass-flow ratio.

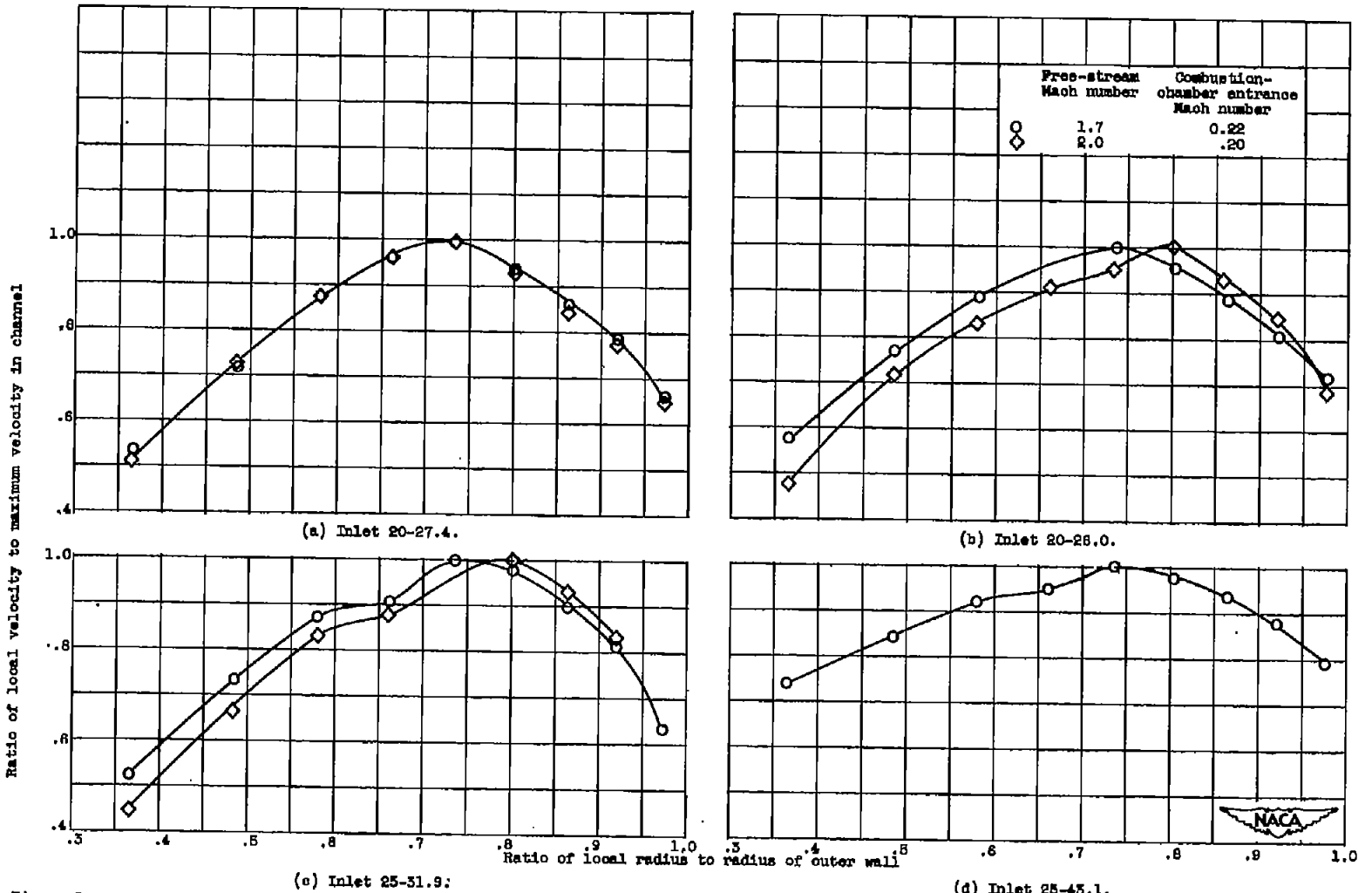

Figure 8. - Effect of inlet type and freestream Mach number on velocity distribution at combustion-chamber entrance. Distributions across upper half of annulus; critical mass flow; angle of attack, 0°.

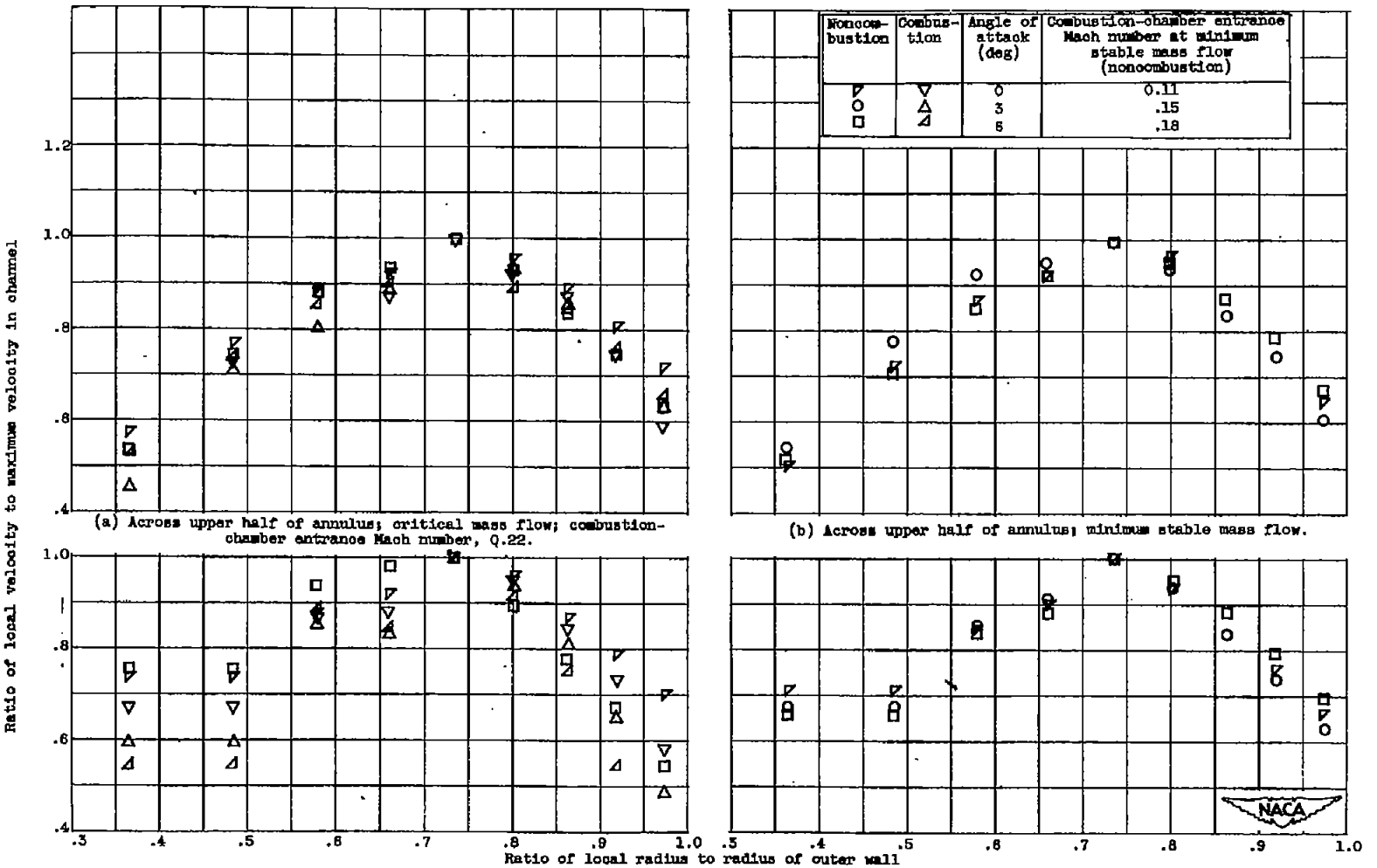

(a) Across upper half of annulus; critical mass flow; combustion-chamber entrance Mach number, 0.22.

(b) Across upper half of annulus; minimum stable mass flow.

(c) Across lower half of annulus; critical mass flow; combustion-chamber entrance Mach number, 0.22.

(d) Across lower half of annulus; minimum stable mass flow.

Figure 9. - Effect of angle of attack, mass-flow ratio, and combustion on velocity distribution at combustion-chamber entrance. Free-stream Mach number, 1.7; inlet 20-26.0.

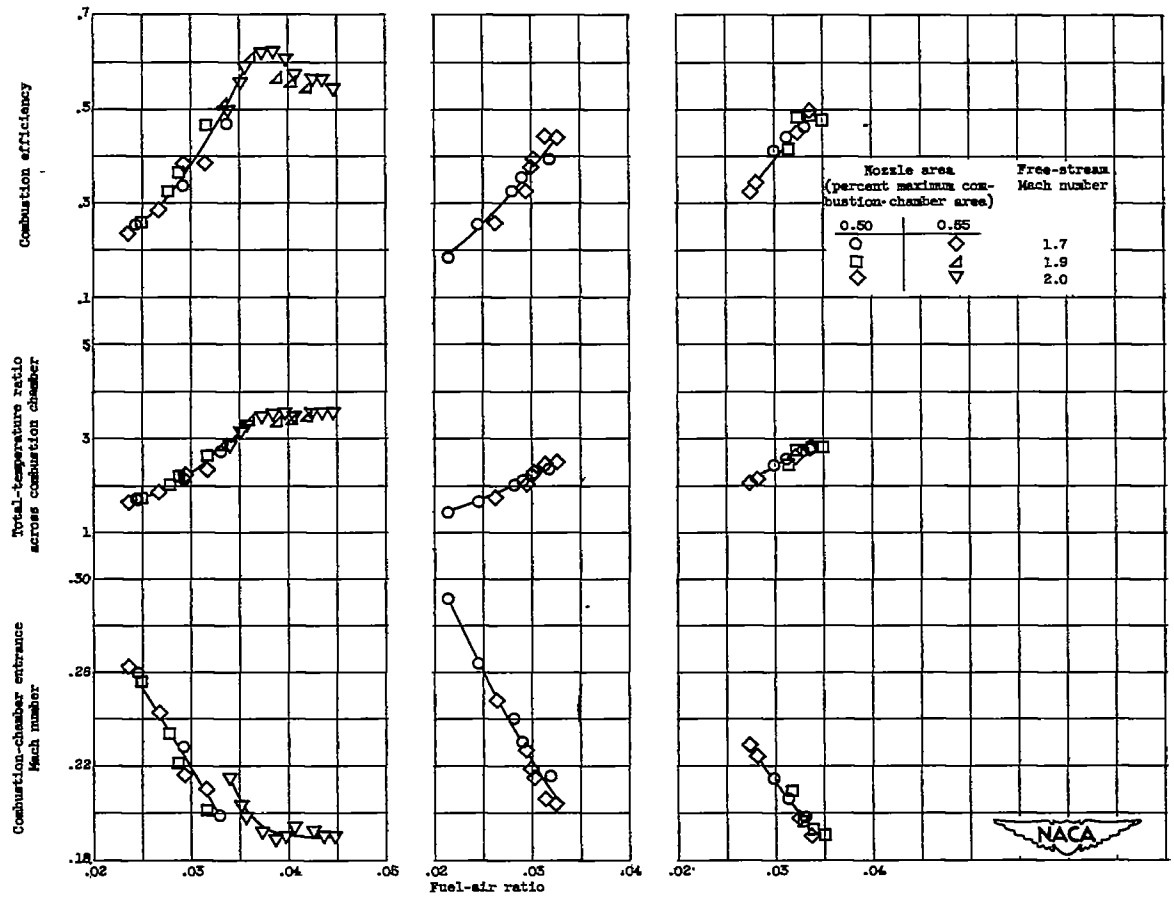

(a) Inlet 20-27.4, ratio of nozzle area to maximum combustion chamber area, 0.50 and 0.55.

(b) Inlet 20-26.2, ratio of nozzle area to maximum combustion chamber area, 0.50.

(c) Inlet 20-26.0, ratio of nozzle area to maximum combustion chamber area, 0.50.

Figure 10. - Variation of combustion efficiency, temperature ratio, and combustion-chamber entrance Mach number with fuel-air ratio at zero angle of attack.

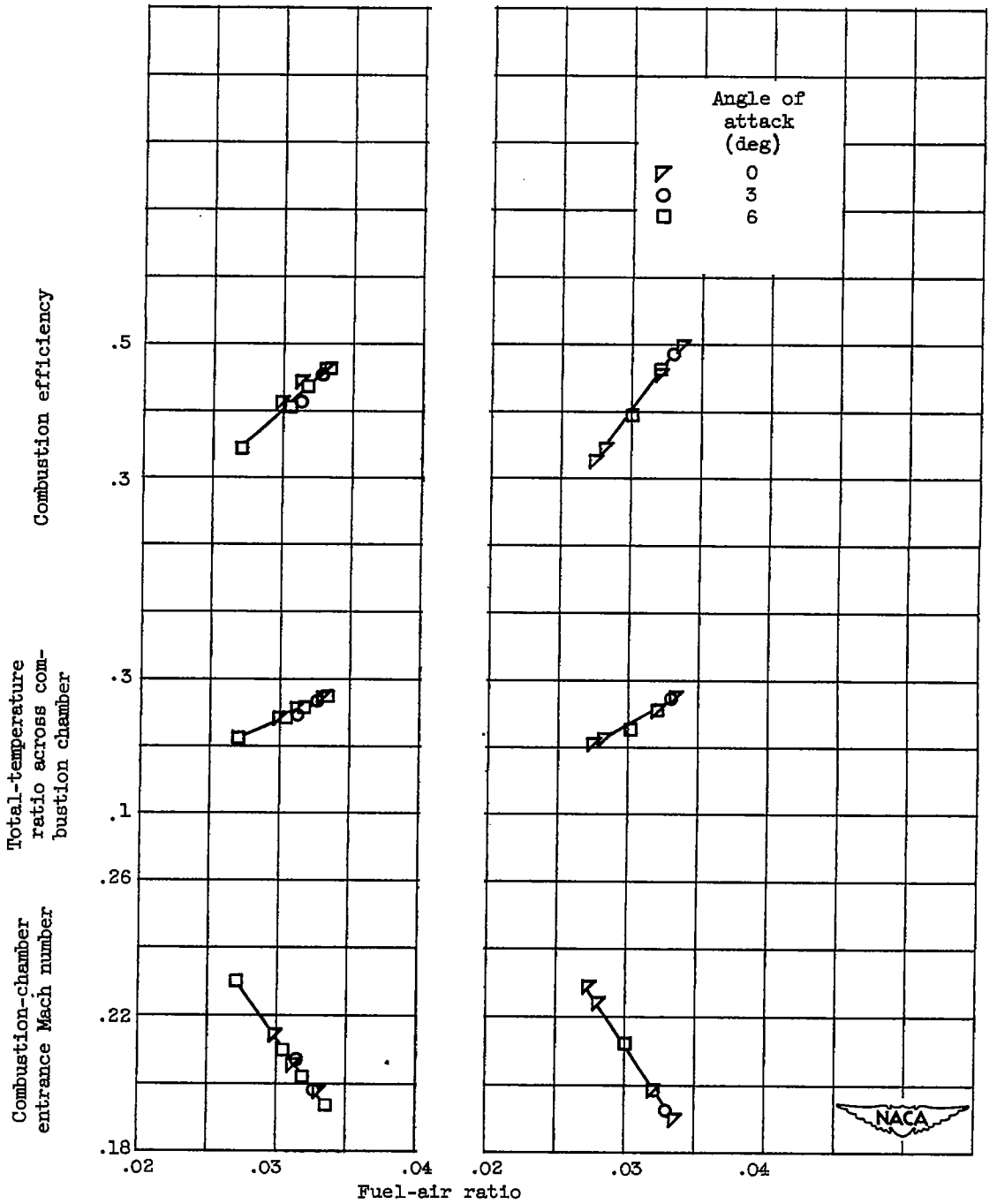

(a) Free-stream Mach number, 1.7.

(b) Free-stream Mach number, 2.0.

Figure 11. - Variation of combustion efficiency, temperature ratio, and combustion-chamber entrance Mach number with fuel-air ratio at various angles of attack; inlet 20-26.0. Ratio of nozzle area to maximum combustion-chamber area, 0.50.

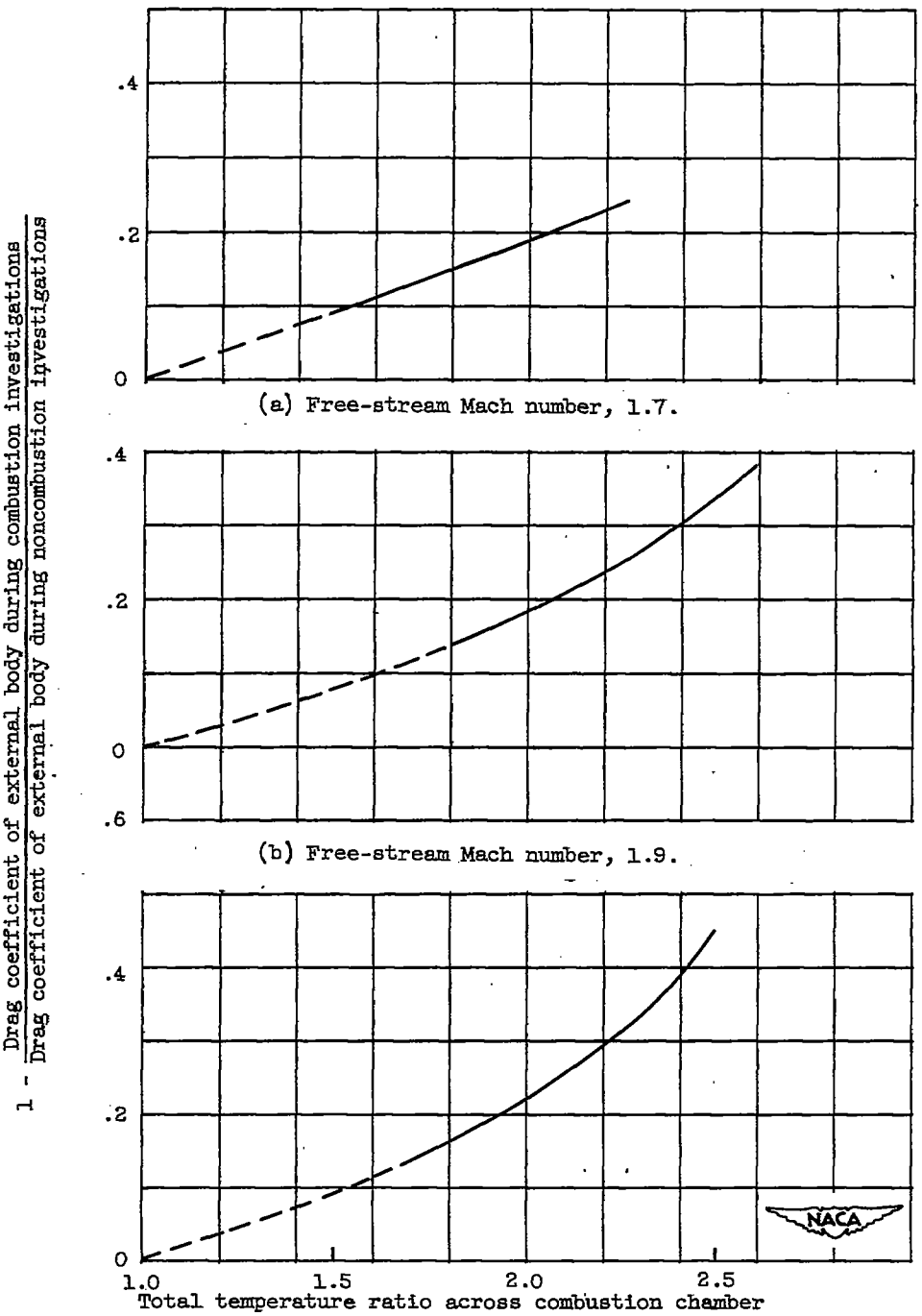

Figure 12. - Effect of temperature on body plus boattail drag coefficient. Ratio of nozzle area to maximum combustion-chamber area, 0.50.

NACA-Langley - 5-5-52 - 325